

1 **Title:** Rationally designed immunogens enable immune focusing to the SARS-CoV-2 receptor
2 binding motif

3

4

5 **Authors:** Blake M. Hauser¹, Maya Sangesland¹, Kerri St. Denis¹, Jared Feldman¹, Evan C. Lam¹,
6 Ty Kannegieter¹, Alejandro B. Balazs¹, Daniel Lingwood¹, Aaron G. Schmidt^{1,2*}

7

8

9 ¹Ragon Institute of MGH, MIT and Harvard, Cambridge, MA, 02139, USA

10

11 ²Department of Microbiology, Harvard Medical School, Boston, MA 02115, USA

12

13

14

15 **Key words:** immunogen design, glycan, immune focusing, SARS-CoV-2, coronavirus

16

17

18

19 **Correspondence:**

20 Aaron G. Schmidt

21 Tel: 857-268-7118; E-mail: aschmidt@crystal.harvard.edu

22

23

24

25 **ABSTRACT**

26 Eliciting antibodies to surface-exposed viral glycoproteins can lead to protective responses that
27 ultimately control and prevent future infections. Targeting functionally conserved epitopes may
28 help reduce the likelihood of viral escape and aid in preventing the spread of related viruses with
29 pandemic potential. One such functionally conserved viral epitope is the site to which a receptor
30 must bind to facilitate viral entry. Here, we leveraged rational immunogen design strategies to
31 focus humoral responses to the receptor binding motif (RBM) on the SARS-CoV-2 spike. Using
32 glycan engineering and epitope scaffolding, we find an improved targeting of the serum response
33 to the RBM in context of SARS-CoV-2 spike imprinting. Furthermore, we observed a robust
34 SARS-CoV-2-neutralizing serum response with increased potency against related sarbecoviruses,
35 SARS-CoV and WIV1-CoV. Thus, RBM focusing is a promising strategy to elicit breadth across
36 emerging sarbecoviruses and represents an adaptable design approach for targeting conserved
37 epitopes on other viral glycoproteins.

38

39 **One Sentence Summary:** SARS-CoV-2 immune focusing with engineered immunogens

40

41 **MAIN TEXT**

42 Humoral responses elicited by vaccination or infection predominantly target surface-exposed viral
43 glycoproteins. These responses can often provide protection against future infections to the same
44 or closely related viral variants. However, in some instances, such as influenza and HIV, the
45 elicited responses are often poorly protective as they target variable epitopes (1, 2). Furthermore,
46 waning of responses (i.e., durability), as is the case for common cold-causing coronaviruses,
47 results in susceptibility to reinfections (3-6). For SARS-CoV-2 (SARS-2) it remains unclear
48 whether current vaccines will confer long-term protection. Furthermore, it is increasingly apparent
49 that humoral immunity elicited by vaccination or natural infection may provide reduced protection
50 against emerging SARS-2 variants (7-9). Thus, implementing rational design strategies aimed at
51 directing the immune response to conserved viral epitopes may help reduce the likelihood of viral
52 escape and lead to more broadly protective responses (10, 11).

53

54 Two immunogen design strategies used to direct humoral responses include “masking” epitopes
55 via engineering putative N-linked glycosylation sites (PNGs) and the design of protein scaffolds
56 to present broadly protective epitopes (12, 13); these strategies have been used previously for viral
57 glycoproteins RSV F, influenza hemagglutinin and HIV envelope (14-16). Applying these
58 approaches to the SARS-2 spike provides an opportunity to potentially improve serum
59 neutralization potency, efficacy against variants, and cross-reactivity of antibody responses. A
60 potential target of these efforts is the angiotensin converting enzyme 2 (ACE2) receptor binding
61 motif (RBM) of the receptor binding domain (RBD) (17, 18). Indeed, several potentially neutralizing
62 RBM-directed antibodies that interfere with ACE2 binding are protective and some can also
63 neutralize related sarbecoviruses (10, 11, 18-20). Here, we show that hyperglycosylation of the
64 RBD and a “resurfacing” approach that grafts the RBM from SARS-2 onto heterologous
65 coronavirus RBDs focuses serum responses to the RBM. This immune-focused response is
66 potentially neutralizing with breadth across SARS-2 variants and other coronaviruses.

67

68 The RBM of SARS-2 and related sarbecoviruses, SARS-CoV (SARS-1) and WIV1-CoV (WIV1),
69 is a contiguous sequence spanning residues 437-507 (SARS-2 numbering) of the spike protein. In
70 an effort to elicit RBM-specific responses only, we first asked whether the RBM itself could be
71 recombinantly expressed in absence of the rest of the RBD (Fig. 1A). While the SARS-2 RBM

72 could indeed be overexpressed, it failed to both engage the conformation-specific RBM-directed
73 antibody B38 and bind to cell-surface expressed ACE2 (**Fig. S1**). These results likely suggest that
74 the RBM is conformationally flexible, and that the RBD serves as a structural “scaffold” to
75 stabilize the RBM in its binding-compatible conformation. To circumvent the considerable hurdle
76 of *de novo* scaffold design for RBM presentation, we asked whether heterologous sarbecovirus
77 RBDs from SARS-1 and WIV1 and the more distantly related merbecovirus MERS-CoV (MERS)
78 could serve as scaffolds (**Fig. 1A**)—variations of this approach were used previously to modulate
79 ACE2 binding properties (21, 22). In context of immunizations, we hypothesized that these
80 heterologous RBDs would present the SARS-2 RBM while removing any other SARS-2-specific
81 epitopes. The SARS-1, WIV-1 and MERS RBDs share a pairwise amino acid identity with SARS-
82 2 of 73.0%, 75.4% and 19.5%, respectively. The RBM is less conserved despite have a shared
83 ACE2 receptor for SARS-1 and WIV1 with only 49.3% and 52.1% identity, respectively; as MERS
84 uses DPP4 as a receptor, its RBM shares no notable identity (23). While we were unable to
85 “resurface” MERS RBD with the SARS-2 RBM, the related SARS-1 and WIV-1 RBDs
86 successfully accepted the RBM transfer. These resurfaced constructs, rsSARS-1 and rsWIV-1
87 retained binding to the SARS-2 RBM-specific B38 antibody as well as effectively engaged ACE2
88 (**Fig. S2**) (19). These data suggest that there are sequence and structural constraints within the
89 RBD required for successful RBM grafting; such an approach may be facilitated by using CoV
90 RBDs that use the same receptor for viral entry.

91

92 We next used these resurfaced RBDs as templates for further modification using glycan
93 engineering. This approach aimed to mask conserved, cross-reactive epitopes shared between the
94 SARS-1, SARS-2, and WIV1 RBDs. There are two evolutionarily conserved PNGs at positions
95 331 and 343; SARS-1 and WIV1 have an additional conserved PNG at position 370 (SARS-2
96 numbering). To further increase overall surface glycan density, we introduced novel PNGs onto
97 wildtype SARS-2 as well as rsSARS-1 and rsWIV1 RBDs. Based on structural modeling, we
98 identified 5 potential sites on rsSARS-1 and rsWIV1 as well as 6 on SARS-2. Including the native
99 PNGs, all constructs had a total of 8 glycans (**Fig. 1B-D, S3**)—we denote these hyperglycosylated
100 (hg) constructs as SARS-2^{hg}, rsSARS-1^{hg}, and rsWIV1^{hg}. We expressed these constructs in
101 mammalian cells to ensure complex glycosylation in order to maximize any glycan “shielding”
102 effect. We subsequently characterized these constructs using the RBM-directed antibody B38, as

103 well as ACE2 binding, to ensure that the engineered PNGs did not adversely affect the RBM
104 conformation. Overall, the hyperglycosylated constructs were largely comparable in affinity for
105 B38, with only ~2-fold decrease, and still effectively engaged ACE2 (**Fig. S4**). These results
106 confirm a conformational and functionally intact RBM.

107

108 Next, we assessed whether the engineered PNGs abrogated binding to sarbecovirus cross-reactive
109 antibodies S309 and CR3022—both antibodies were isolated from SARS-1 convalescent
110 individuals (24, 25). The CR3022 contact residues on SARS-1 and WIV1 differ only at a single
111 residue while SARS-2 differs at 5 residues across both CR3022 and S309 epitopes (26).
112 Importantly, these epitopic regions were shown to be a significant portion of the SARS-2 RBD-
113 directed response in murine immunizations and thus any RBM focusing would require masking of
114 these regions (**Fig. S4**) (24, 25, 27). While SARS-2^{hg} effectively abrogated S309 and CR3022
115 binding, the engineered PNGs at the antibody:antigen interface on rsSARS-1^{hg} and rsWIV1^{hg} did
116 not completely abrogate S309 and CR3022 binding. We therefore incorporated unique mutations
117 on rsSARS-1^{hg} and rsWIV1^{hg} so that any elicited antibodies would be less likely to cross-react
118 between these two constructs. To that end, we found K378A and the engineered glycan at residue
119 383 (SARS-2 numbering) completely abrogated CR3022 binding in both rsSARS-1^{hg} and
120 rsWIV1^{hg} (**Fig. S4**). For S309, mutations P337D in rsSARS-1^{hg} and G339W in rsWIV1^{hg} in
121 addition to glycans at residues 441 and 354 (SARS-2 numbering) were sufficient to disrupt binding
122 (**Fig. S4**). We made two additional mutations, G381R, M430K on rsSARS-1^{hg} and K386A, T430R
123 on rsWIV1^{hg}, to further increase the antigenic distance between these scaffolds (**Fig. 1C, D**).

124

125 We then tested the immunogenicity and antigenicity of our optimized constructs and assessed their
126 RBM immune-focusing properties, in the murine model. In order to increase avidity and to
127 minimize any off-target tag-specific responses, we generated trimeric versions of each immunogen
128 using our previously characterized hyperglycosylated, cysteine-stabilized GCN4 tag (*hgGCN4^{cys}*)
129 (27, 28). We first primed all cohorts with SARS-2 spike to reflect pre-existing SARS-2 immunity
130 and to imprint an initial RBM response that may be recalled and selectively expanded by our
131 immunogens. To test potential RBM immune-focusing, one cohort was sequentially immunized
132 with SARS-2^{hg} trimers (“Trimer^{hg} cohort”) and a second cohort was immunized with SARS-2^{hg}
133 trimers followed by a cocktail of rsSARS-1^{hg} and rsWIV1^{hg} (“Cocktail^{hg} cohort”) (**Fig. 2A**). In

134 order to facilitate comparisons and establish the efficacy of RBM-focusing, we included a “ Δ RBM
135 cohort”. This cohort was immunized with a modified SARS-2 RBD (Δ RBM) with four novel
136 glycans engineered at positions 448, 475, 496, and 501 within the RBM. These PNGs effectively
137 abrogate RBM-directed B38 antibody binding and engagement of ACE2 (27) and should restrict
138 elicited humoral response to this epitope. Finally, as a control cohort, we included a SARS-2 spike
139 prime followed with sequential immunizations with wildtype (i.e., unmodified) SARS-2 RBD
140 trimer (“Trimer cohort”).

141
142 Overall, we find that all cohorts elicit robust serum responses to wildtype SARS-2 RBD (**Fig. 2B-**
143 **C, S5**). In order to specifically evaluate the RBM-directed responses, we compared serum ELISA
144 titers to wildtype SARS-2 RBD and the SARS-2 Δ RBM RBD construct. We find that the Trimer^{hg}
145 and Cocktail^{hg} cohorts had a significant increase in serum titers to wildtype SARS-2 RBD relative
146 to SARS-2 Δ RBM RBD; this was in contrast to the Δ RBM and Trimer cohorts (**Fig. 2B,C, S5A,B**).
147 Across the Trimer^{hg} and Cocktail^{hg} cohorts, the median binding loss to the SARS-2 Δ RBM RBD
148 relative to wildtype SARS-2 RBD was 82%, indicating that ~82% of serum antibodies are RBM-
149 directed by this metric. The Cocktail^{hg} cohort had a slight increase in RBM focusing relative to the
150 Trimer^{hg} cohort which received two SARS-2^{hg} boosts. This observed increase may be due to
151 increasing the overall antigenic distance (i.e., sequence difference) between the WIV1 and SARS-
152 1 RBDs relative to SARS-2 while maintaining the identical SARS-2 RBM epitope. Additionally,
153 we find that the Trimer^{hg} and Cocktail^{hg} cohorts had significantly lower titers to SARS-1 and WIV1
154 RBDs as compared to SARS-2 RBD (**Fig. 2B**). This difference was most pronounced in the
155 Cocktail^{hg} cohort, suggesting that the hyperglycosylation and engineered mutations within the
156 RBD effectively dampened responses to these conserved, cross-reactive epitopes that are present
157 outside the RBM and shared between SARS-1, WIV1, and SARS-2. Furthermore, serum titers
158 against the rsSARS-1 and rsWIV1 RBDs were comparable to SARS-2 RBD, indicating that there
159 is minimal antibody response directed towards wildtype SARS-1 and WIV1 RBD epitopes in
160 comparison to the SARS-2 RBM (**Fig. 2D, S5C**). We observed no significant glycan-dependent
161 serum response in either cohort that used hyperglycosylation (**Fig. S6**). Collectively, these data
162 confirm an enhanced SARS-2 RBM-focused serum response elicited by our engineered
163 immunogens.

164

165 We next compared the neutralization potency of all cohorts using SARS-1, SARS-2, and WIV1
166 pseudoviruses (29, 30). While all cohorts elicited a potent SARS-2 neutralizing response, notably,
167 the Trimer^{hg} and Cocktail^{hg} cohorts also exhibited potent SARS-1 and WIV1 pseudovirus
168 neutralization relative to the control cohorts (**Fig. 3A, S7, S5B**). This is particularly noteworthy
169 for the Trimer^{hg} cohort as it did not include SARS-1 or WIV1 RBDs in the immunization regimen.
170 WIV1 in this instance is broadly representative of possible future emerging sarbecoviruses with
171 pandemic potential (31). To further epitope map the RBM-focused responses, we performed
172 ELISA-based antibody competition using cross-reactive antibodies CR3022, S309, ADI-55689,
173 and ADI-56046 and WIV1 RBD (**Fig. 3B-C**). The latter two antibodies bind a conserved
174 sarbecovirus RBM epitope also targeted by the antibody ADG-2, which is currently in clinical
175 development (10, 11). Competition ELISAs suggest that the cross reactive WIV1-directed
176 responses in the Trimer^{hg} and Cocktail^{hg} cohorts focus to the ADG-2-like epitope, as well as to the
177 CR3022 and S309 epitopes in the Cocktail^{hg} cohort (**Fig. 3B-C**). Thus, SARS-2^{hg}, rsSARS-1^{hg},
178 and rsWIV1^{hg} RBDs can induce not only potent SARS-2 neutralizing antibodies, but also cross-
179 reactive antibodies that bind to a conserved RBM epitope (**Fig. S8**). Notably, these results are in
180 contrast to our previous work showing that a cocktail of sarbecovirus that included SARS-1 and
181 WIV1 RBDs could predominantly focus the antibody response towards the conserved CR3022
182 and S309 epitopic regions (27).

183
184 Many SARS-2 variants of concern include mutations within the RBM including B.1.1.7, B.1.351
185 and P.1 first detected in the United Kingdom, South Africa, and Brazil, respectively (**Fig. 4A**). We
186 therefore asked what the consequence was of enhanced focusing to the RBM and whether the
187 elicited responses elicited were sensitive to these mutations. Interestingly, serum from the Trimer^{hg}
188 and Cocktail^{hg} cohorts showed no significant loss of binding to the B.1.351 RBD compared to the
189 wildtype SARS-2 RBD (**Fig. 4A, B**). This is in contrast to the control Trimer cohort, which showed
190 a significant loss of binding and parallels the observation of reduced serum binding from human
191 subjects immunized with current SARS-2 vaccines (9, 32, 33). Second, we tested all sera for
192 neutralization against SARS-2 variant pseudoviruses: B.1.1.7, B.1.351 and P.1. While the control
193 Trimer cohort could still neutralize P.1 and B.1.1.7 pseudoviruses, there was a significant loss of
194 neutralization to the B.1.351 variant, consistent with our ELISA data. In contrast, we find no
195 significant loss of neutralization against these variants in the Trimer^{hg}, Cocktail^{hg}, and Δ RBM

196 cohorts (**Fig. 4C**). For Δ RBM cohort, the elicited responses were likely focused to neutralizing
197 epitopes within the RBD (e.g., CR3022, S309) and therefore were not sensitive to these RBM
198 mutations. However, the neutralizing response observed in Trimer^{hg} and Cocktail^{hg} cohorts
199 potentially indicate that immune-focusing to the RBM may allow for greater recognition (i.e.,
200 accommodation) of mutations compared to the RBM-directed antibody response elicited via
201 infection or vaccination (32, 34).

202

203 Collectively, our results demonstrate immunogen design approaches that can be leveraged to
204 enhance an RBM-focused humoral response. It is a strategy that maintains protective SARS-2
205 neutralization while also eliciting humoral responses that recognize emerging variants and
206 coronaviruses with pandemic potential. Importantly, these design strategies are not limited to
207 coronaviruses and are adaptable to other viruses as a general approach to elicit protective responses
208 to conserved epitopes.

209

210 **Acknowledgments:** We thank members of the Schmidt Laboratory for helpful discussions. We
211 thank Timothy Caradonna and Catherine Jacob-Dolan for critical reading of the manuscript. We
212 thank Dr. Jason McLellan from University of Texas, Austin for the spike plasmid. We thank Nir
213 Hacoheh and Michael Farzan for the kind gift of the ACE2 expressing 293T cells.

214

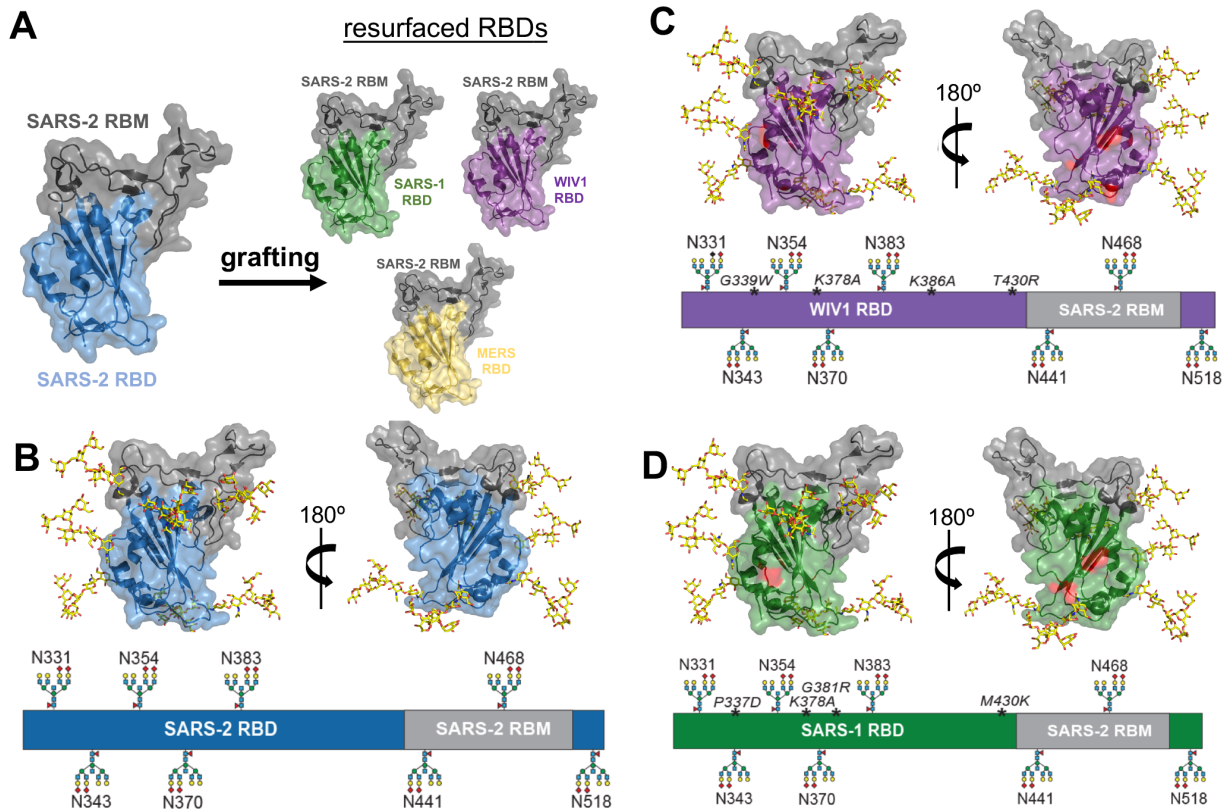
215 **Funding:** We acknowledge funding from NIH R01s AI146779 (AGS), AI124378, AI137057 and
216 AI153098 (DL), and a Massachusetts Consortium on Pathogenesis Readiness (MassCPR) grant
217 (AGS); training grants: NIGMS T32 GM007753 (BMH and TMC); T32 AI007245 (JF); F31
218 AI138368 (MS). A.B.B. is supported by the National Institutes for Drug Abuse (NIDA) Avenir
219 New Innovator Award DP2DA040254, the MGH Transformative Scholars Program as well as
220 funding from the Charles H. Hood Foundation (ABB). This independent research was supported
221 by the Gilead Sciences Research Scholars Program in HIV (ABB).

222

223

224 **Author contributions:** Conceptualization, BMH, AGS; Methodology, BMH, ECL, ABB, DL,
225 AGS; Investigation, BMH, MS, KS, ECL, JF, TK; Writing – Original Draft, BMH and AGS;
226 Writing – Review and Editing, all authors; Funding Acquisition, ABB, DL, AGS; Supervision,
227 ABB, DL, AGS.; **Competing interests:** Authors declare no competing interests.; and **Data and**
228 **materials availability:** All data is available in the main text or in the supplementary materials.

229



230

231

232 **Fig. 1. Resurfacing and hyperglycosylation approaches for immune-focusing. (A)** Design

233 schematic for resurfacing SARS-1 (rsSARS-1 and WIV1 (rsWIV1

234) with the SARS-2 receptor binding motif (RBM). Design schematic for hyperglycosylating

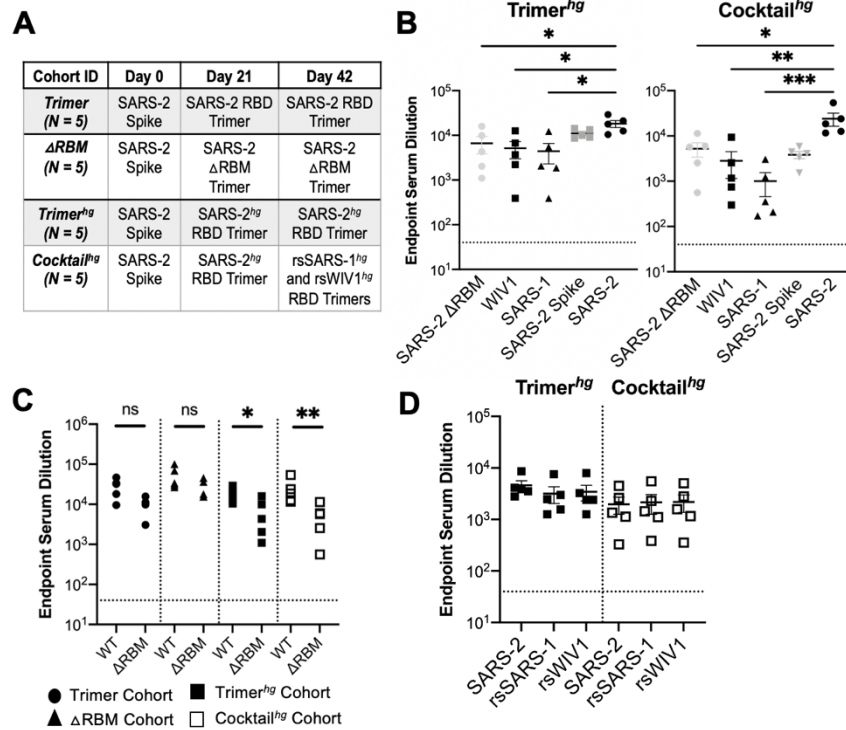
235 SARS-2 (B), rsSARS-1 (C) and rsWIV1 (D) receptor binding domains (RBDs). Non-native

236 engineered glycans and native glycans are modeled; native SARS-2 RBM glycan at position 331

237 is omitted in the schematic. Mutations in the WIV1 and SARS-1 RBDs are shown in red and

238 italicized in the linear diagram. All images were created using PDB 6M0J.

239



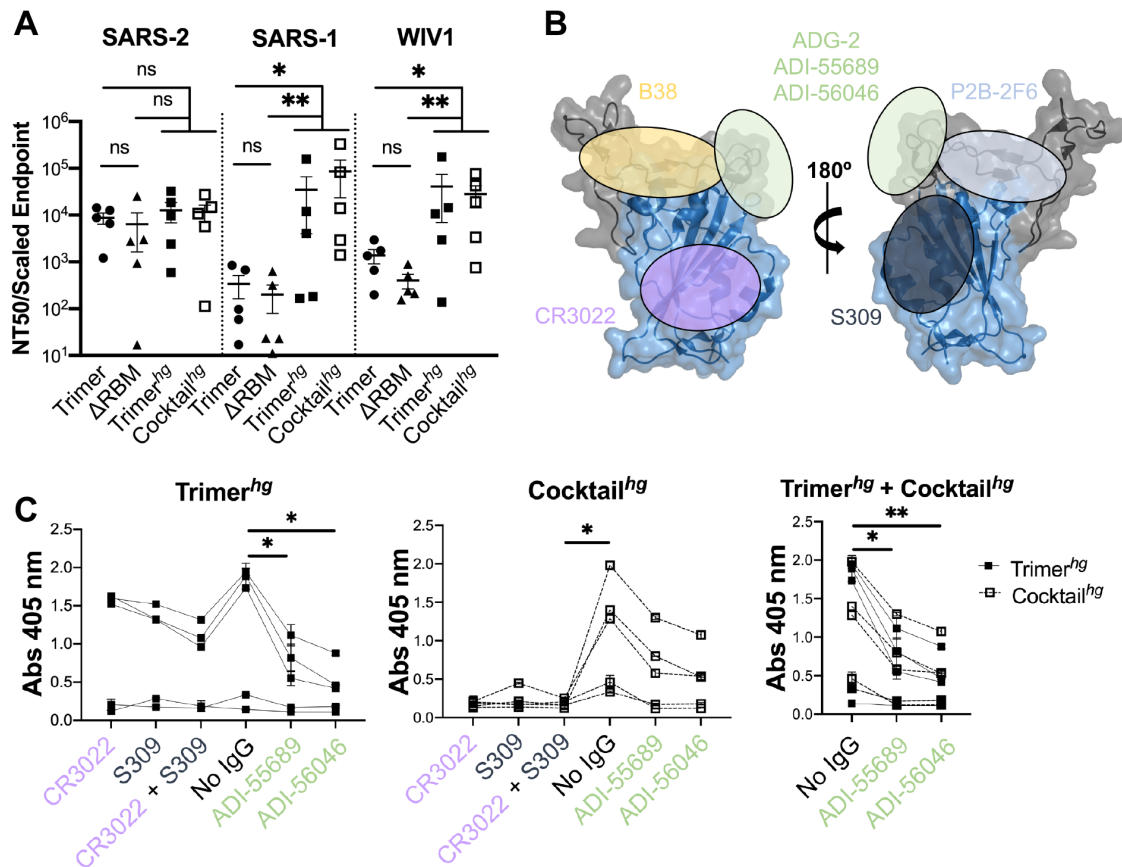
240

241

242 **Fig. 2. Serum analysis from cohorts.** (A) Schematic of immunization cohorts; N= number of
 243 mice in each cohort (B, C) Serum following immunizations was assayed in ELISA at day 56 with
 244 different coronavirus antigens. Statistical significance was determined using Kruskal-Wallis test
 245 with post-hoc analysis using Dunn's test corrected for multiple comparisons or Mann-Whitney U
 246 test (* = $p < 0.05$, ** = $p < 0.01$, *** = $p < 0.001$). (D) Day 56 serum samples assayed against
 247 rsSARS-1 and rsWIV1 RBDs no longer show statistically significant differences in binding
 248 compared to SARS-2 RBD as determined using Kruskal-Wallis test with post-hoc analysis using
 249 Dunn's test corrected for multiple comparisons.

250

251



252

253

254 **Fig. 3. Potency and characterization of SARS-like coronavirus neutralization response. (A)**

255 Day 56 serum from all mice was assayed for neutralization against SARS-2, SARS-1, and WIV1

256 pseudoviruses. Statistical significance was determined using the Kruskal-Wallis test with post-hoc

257 analysis using Dunn's test corrected for multiple comparisons (* = $p < 0.05$, ** = $p < 0.01$, ns =

258 not significant). **(B)** Approximate locations of representative antibody epitopes from each of the

259 four SARS-2 RBD-directed antibody classes (*18*) and ADG-2-like antibodies on the SARS-2

260 RBD. (PDB: 6M0J) **(C)** Antibody competition ELISAs with WIV1 RBD as the coating antigen.

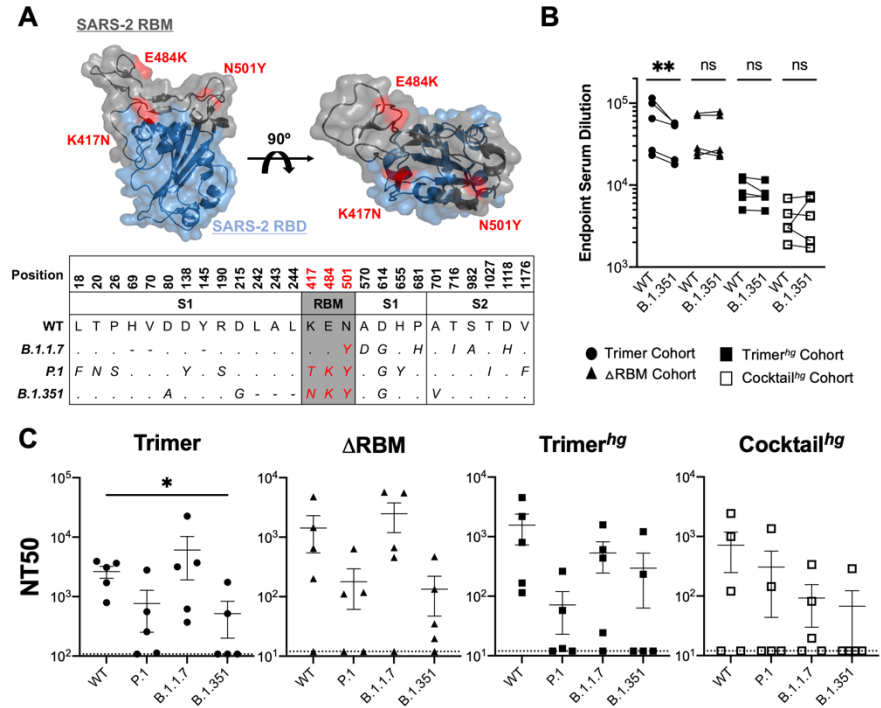
261 The Trimer^{hg} and Cocktail^{hg} were independently analyzed (first two panels) and statistically

262 combined (last panel) to highlight observed RBM-focusing. Statistical significance was

263 determined the Friedman test with post-hoc analysis using Dunn's test corrected for multiple

264 comparisons (* = $p < 0.05$, ** $p < 0.01$).

265



266
267

268 **Fig. 4. Binding and neutralization of SARS-2 variants.** (A) Structural depiction of SARS-2
 269 variant RBD mutations for 501Y.V2 (red), as well as ACE2 contact residues (cyan). (PDB: 6M0J)
 270 Sequences depict all spike mutations across select variants. (B) Day 56 serum was assayed in
 271 ELISA against SARS-2 RBD (WT) and SARS-2 RBD with K417N, E484K, and N501Y mutations
 272 (B.1.351). Statistical significance was determined using the ratio paired t-test (* = $p < 0.05$, ** =
 273 $p < 0.01$; ns = not significant). (C) Day 56 serum was assayed against SARS-2 variant
 274 pseudoviruses for neutralization. Statistical significance was determined using the Kruskal-Wallis
 275 test with post-hoc analysis using Dunn's test corrected for multiple comparisons (* = $p < 0.05$).
 276 Lower limit of detection for each cohort is shown with a dotted line, and y-axis values were
 277 selected accordingly. Pseudovirus neutralization for WT SARS-2 was also performed with the
 278 $\sim 10^2$ limit of detection for the Δ RBM, Trimer^{hg}, and Cocktail^{hg} cohorts (Fig. S7), but NT50 values
 279 at the limit of detection were adjusted to match the lower limit of detection ($\sim 10^1$) for the variant
 280 pseudoviruses to facilitate fair comparison.

281

282 **METHODS**

283

284 Immunogen and Coating Protein Expression and Purification

285 The SARS-CoV-2 (Genbank MN975262.1), SARS-CoV (Genbank ABD72970.1), WIV1-CoV
286 (Genbank AGZ48828.1) RBDs were used as the basis for constructing these immunogens. To graft
287 the SARS-2 RBM onto SARS-1 and WIV1 scaffolds to create the rsSARS-1 and rsWIV1
288 monomers, boundaries of SARS-2 residues 437 – 507 were used. All constructs were codon
289 optimized by Integrated DNA Technologies and purchased as gblocks. Gblocks were then cloned
290 into pVRC and sequence confirmed via Genewiz. Monomeric constructs for serum ELISA coating
291 contained C-terminal HRV 3C-cleavable 8xHis and SBP tags. Trimeric constructs also included
292 C-terminal HRV 3C-cleavable 8xHis tags, in addition to a previously published hyperglycosylated
293 GCN4 tag with two engineered C-terminal cystines (27, 28). Dr. Jason McLellan at the University
294 of Texas, Austin provided the spike plasmid, which contained a non-cleavable foldon trimerization
295 domain in addition to C-terminal HRV 3C cleavable 6xHis and 2xStrep II tags. The SARS-2
296 Δ RBM RBD construct was generated as previously described with four additional engineered
297 putative N-linked glycosylation sites at positions 448, 475, 496, and 501 (27).

298

299 Expi 293F cells (ThermoFisher) were used to express proteins. Transfections were performed with
300 Expifectamine reagents per the manufacturer's protocol. After 5-7 days, transfections were
301 harvested and centrifuged for clarification. Cobalt-TALON resin (Takara) was used to perform
302 immobilized metal affinity chromatography via the 8xHis tag. Proteins were eluted using
303 imidazole, concentrated, and passed over a Superdex 200 Increase 10/300 GL (GE Healthcare)
304 size exclusion column. Size exclusion chromatography was performed in PBS (Corning). For
305 immunogens, HRV 3C protease (ThermoScientific) cleavage of affinity tags was performed prior
306 to immunization. Cobalt-TALON resin was used for a repurification to remove the His-tagged
307 HRV 3C protease, cleaved tag, and remaining uncleaved protein.

308

309 Fab and IgG Expression and Purification

310 The variable heavy and light chain genes for each antibody were codon optimized by Integrated
311 DNA Technologies, purchased as gblocks, and cloned into pVRC constructs which already
312 contained the appropriate constant domains as previously described (35, 36). The Fab heavy chain

313 vector contained a HRV 3C-cleavable 8xHis tag, and the IgG heavy chain vector contained HRV
314 3C-cleavable 8xHis and SBP tags. The same transfection and purification protocol as used for the
315 immunogens and coating proteins was used for the Fabs and IgGs.

316

317 Biolayer Interferometry

318 Biolayer interferometry (BLI) experiments were performed using a BLItz instrument (Fortebio)
319 with FAB2G biosensors (Fortebio). All proteins were diluted in PBS. Fabs were immobilized to
320 the biosensors, and coronavirus proteins were used as the analytes. To determine binding affinities,
321 single-hit measurements were performed starting at 10 μ M to calculate an approximate K_D in order
322 to evaluate which concentrations should be used for subsequent titrations. Measurements at a
323 minimum of three additional concentrations were performed. Vendor-supplied software was used
324 to generate a final K_D estimate via a global fit model with a 1:1 binding isotherm.

325

326 Immunizations

327 All immunizations were performed using female C57BL/6 mice (Jackson Laboratory) aged 6-10
328 weeks. Mice received 20 μ g of protein adjuvanted with 50% w/v Sigma adjuvant in 100 μ L of
329 inoculum via the intraperitoneal route. Following an initial prime (day 0), boosts occurred at days
330 21 and 42. Serum samples were collected for characterization on day 56 from all cohorts, in
331 addition to day 35 for the HG Trimer and HG Cocktail cohorts. All experiments were conducted
332 with institutional IACUC approval (MGH protocol 2014N000252).

333

334 Serum ELISAs

335 Serum ELISAs were executed using 96-well, clear, flat-bottom, high bind microplates (Corning).
336 These plates were coated with 100 μ L of protein, which were adjusted to a concentration of 5
337 μ g/mL (in PBS). Plates were incubated overnight at 4°C. After incubation, plates had their coating
338 solution removed and were blocked using 1% BSA in PBS with 1% Tween. This was done for 60
339 minutes at room temperature. This blocking solution was removed, and sera was diluted 40-fold
340 in PBS. A 5-fold serial dilution was then performed. CR3022 IgG, similarly serially diluted (5-
341 fold) from a 5 μ g/mL starting concentration, was used as a positive control. 40 μ L of primary
342 antibody solution was used per well. Following this, samples were incubated for 90 minutes at
343 room temperature. Plates were washed three times using PBS-Tween. 150 μ L of HRP-conjugated

344 rabbit anti-mouse IgG antibody, sourced commercially from Abcam (at a 1:20,000 dilution in
345 PBS), was used for the secondary incubation. Secondary incubation was performed for one hour,
346 similarly at room temperature. Plates were subsequently washed three times using PBS-Tween.
347 1xABTS development solution (ThermoFisher) was used according to the manufacturer's
348 protocol. Development was abrogated after 30 minutes using a 1% SDS solution, and plates were
349 read using a SpectraMaxiD3 plate reader (Molecular Devices) for absorbance at 405 nm.

350

351 Competition ELISAs

352 A similar protocol to the serum ELISAs was used for the competition ELISAs. For the primary
353 incubation, 40 μ L of the relevant IgG at 1 μ M was used at room temperature for 60 minutes. Mouse
354 sera were then spiked in such that the final concentration of sera fell within the linear range for the
355 serum ELISA titration curve for the respective coating antigen, and an additional 60 minutes of
356 room temperature incubation occurred. After removing the primary solution, plates were washed
357 three times with PBS-Tween. Secondary incubation consisted of HRP-conjugated goat anti-mouse
358 IgG, human/bovine/horse SP ads antibody (Southern Biotech) at a concentration of 1:4000. The
359 remaining ELISA procedure (secondary incubation, washing, developing) occurred as described
360 for the serum ELISAs.

361

362 ACE2 Cell Binding Assay

363 ACE2 expressing 293T cells (37) (a kind gift from Nir Hacohen and Michael Farzan) were
364 harvested. A wash was performed using PBS supplemented with 2% FBS. 200,000 cells were
365 allocated to each labelling condition. Primary incubation occurred using 100 μ L of 1 μ M antigen
366 in PBS on ice for 60 minutes. Two washes were performed with PBS supplemented with 2% FBS.
367 Secondary incubation was performed using 50 μ L of 1:200 streptavidin-PE (Invitrogen) on ice for
368 30 mins. Two washes were performed with PBS supplemented with 2% FBS, and then cells were
369 resuspended in 100 μ L of PBS supplemented with 2% FBS. A Stratadigm S1000Exi Flow
370 Cytometer was used to perform flow cytometry. FlowJo (version 10) was used to analyze FCS
371 files.

372

373 Pseudovirus Neutralization Assay

374 Serum neutralization against SARS-CoV-2, SARS-CoV, and WIV1-CoV was assayed using
375 pseudotyped lentiviral particles expressing spike proteins described previously (29). Transient
376 transfection of 293T cells was used to generate lentiviral particles. Viral supernatant titers were
377 measured using flow cytometry of 293T-ACE2 cells (37) and utilizing the HIV-1 p24^{CA} antigen
378 capture assay (Leidos Biomedical Research, Inc.). 384-well plates (Grenier) were used to perform
379 assays on a Tecan Fluent Automated Workstation. For mouse sera, samples underwent primary
380 dilutions of 1:3 or 1:9 followed by serial 3-fold dilutions. 20 µL each of sera and pseudovirus (125
381 infectious units) were loaded into each well. Plates were then incubated for 1 hour at room
382 temperature. Following incubation, 10,000 293T-ACE2 cells (37) in 20 µL of media containing
383 15 µg/mL polybrene was introduced to each well. The plates were then further incubated at 37°C
384 for 60-72 hours.

385
386 Cells were lysed using assay buffers described previously (38). Luciferase expression was
387 quantified using a Spectramax L luminometer (Molecular Devices). Neutralization percentage for
388 each concentration of serum was calculated by deducting background luminescence from cells-
389 only sample wells and subsequently dividing by the luminescence of wells containing both virus
390 and cells. Nonlinear regressions were fitted to the data using GraphPad Prism (version 9), allowing
391 IC₅₀ values to be calculated via the interpolated 50% inhibitory concentration. IC₅₀ values were
392 calculated with a neutralization values greater than or equal to 80% at maximum serum
393 concentration for each sample. NT₅₀ values were then calculated using the reciprocal of IC₅₀
394 values. Serum neutralization potency values were calculated by dividing the NT₅₀ against a
395 particular pseudovirus by the endpoint titer against the respective RBD. For samples with NT₅₀
396 values below the limit of detection, the lowest limit of detection across all neutralization assays
397 was used as the NT₅₀ value to calculate neutralization potency. This prevents a higher limit of
398 detection from skewing neutralization potency results. Endpoint titers were normalized relative to
399 a CR3022 IgG control, which was run in every serum ELISA.

400
401 In comparing NT₅₀ values for the various cohorts across the wildtype and variant pseudoviruses,
402 the lowest limit of detection across all neutralization assays performed for a given cohort was used
403 for any NT₅₀ values that fell below the limit of detection. This prevents a higher limit of detection
404 in some assays from skewing the comparison results.

405

406 Statistical Analysis

407 Curve fitting and statistical analyses were performed with GraphPad Prism (version 9). Non-
408 parametric statistics were used throughout. To compare multiple populations, the Kruskal-Wallis
409 non-parametric ANOVA was used with post hoc analysis using Dunn's test for multiple
410 comparisons. The Mann-Whitney U test was used to compare two populations without
411 consideration for paired samples. The ratio-paired t-test was used to compare two populations with
412 consideration for paired samples and evidence of normality. P values in ANOVA analyses were
413 corrected for multiple comparisons. A p value < 0.05 was considered significant.

414 **REFERENCES**

415

- 416 1. J. Overbaugh, L. Morris, The Antibody Response against HIV-1. *Cold Spring Harb*
417 *Perspect Med* **2**, a007039 (2012).
- 418 2. F. Krammer, The human antibody response to influenza A virus infection and
419 vaccination. *Nat Rev Immunol* **19**, 383-397 (2019).
- 420 3. K. A. Callow, H. F. Parry, M. Sergeant, D. A. Tyrrell, The time course of the immune
421 response to experimental coronavirus infection of man. *Epidemiol Infect* **105**, 435-446
422 (1990).
- 423 4. J. O. Hendley, H. B. Fishburne, J. M. Gwaltney, Jr., Coronavirus infections in working
424 adults. Eight-year study with 229 E and OC 43. *Am Rev Respir Dis* **105**, 805-811 (1972).
- 425 5. A. S. Monto, S. K. Lim, The Tecumseh study of respiratory illness. VI. Frequency of and
426 relationship between outbreaks of coronavirus infection. *J Infect Dis* **129**, 271-276
427 (1974).
- 428 6. R. Eguia *et al.*, A human coronavirus evolves antigenically to escape antibody immunity.
429 *bioRxiv*, (2020).
- 430 7. C. K. Wibmer *et al.*, SARS-CoV-2 501Y.V2 escapes neutralization by South African
431 COVID-19 donor plasma. *bioRxiv*, (2021).
- 432 8. P. Wang *et al.*, Increased Resistance of SARS-CoV-2 Variants B.1.351 and B.1.1.7 to
433 Antibody Neutralization. *bioRxiv*, (2021).
- 434 9. Z. Wang *et al.*, mRNA vaccine-elicited antibodies to SARS-CoV-2 and circulating
435 variants. *bioRxiv*, (2021).
- 436 10. A. Z. Wec *et al.*, Broad neutralization of SARS-related viruses by human monoclonal
437 antibodies. *Science* **369**, 731-736 (2020).
- 438 11. C. G. Rappazzo *et al.*, Broad and potent activity against SARS-like viruses by an
439 engineered human monoclonal antibody. *Science* **371**, 823-829 (2021).
- 440 12. G. Bajic *et al.*, Influenza Antigen Engineering Focuses Immune Responses to a
441 Subdominant but Broadly Protective Viral Epitope. *Cell Host Microbe* **25**, 827-835 e826
442 (2019).
- 443 13. G. Bajic *et al.*, Structure-Guided Molecular Grafting of a Complex Broadly Neutralizing
444 Viral Epitope. *ACS Infect Dis* **6**, 1182-1191 (2020).
- 445 14. M. Crispin, A. B. Ward, I. A. Wilson, Structure and Immune Recognition of the HIV
446 Glycan Shield. *Annu Rev Biophys* **47**, 499-523 (2018).
- 447 15. G. Ofek *et al.*, Elicitation of structure-specific antibodies by epitope scaffolds. *Proc Natl*
448 *Acad Sci U S A* **107**, 17880-17887 (2010).
- 449 16. B. E. Correia *et al.*, Proof of principle for epitope-focused vaccine design. *Nature* **507**,
450 201-206 (2014).
- 451 17. L. Piccoli *et al.*, Mapping Neutralizing and Immunodominant Sites on the SARS-CoV-2
452 Spike Receptor-Binding Domain by Structure-Guided High-Resolution Serology. *Cell*
453 **183**, 1024-1042 e1021 (2020).
- 454 18. C. O. Barnes *et al.*, SARS-CoV-2 neutralizing antibody structures inform therapeutic
455 strategies. *Nature* **588**, 682-687 (2020).
- 456 19. Y. Wu *et al.*, A noncompeting pair of human neutralizing antibodies block COVID-19
457 virus binding to its receptor ACE2. *Science* **368**, 1274-1278 (2020).
- 458 20. J. Hansen *et al.*, Studies in humanized mice and convalescent humans yield a SARS-
459 CoV-2 antibody cocktail. *Science* **369**, 1010-1014 (2020).

- 460 21. M. Letko, A. Marzi, V. Munster, Functional assessment of cell entry and receptor usage
461 for SARS-CoV-2 and other lineage B betacoronaviruses. *Nat Microbiol* **5**, 562-569
462 (2020).
- 463 22. J. Shang *et al.*, Structural basis of receptor recognition by SARS-CoV-2. *Nature* **581**,
464 221-224 (2020).
- 465 23. V. S. Raj *et al.*, Dipeptidyl peptidase 4 is a functional receptor for the emerging human
466 coronavirus-EMC. *Nature* **495**, 251-254 (2013).
- 467 24. D. Pinto *et al.*, Cross-neutralization of SARS-CoV-2 by a human monoclonal SARS-CoV
468 antibody. *Nature* **583**, 290-295 (2020).
- 469 25. M. Yuan *et al.*, A highly conserved cryptic epitope in the receptor binding domains of
470 SARS-CoV-2 and SARS-CoV. *Science* **368**, 630-633 (2020).
- 471 26. N. C. Wu *et al.*, A natural mutation between SARS-CoV-2 and SARS-CoV determines
472 neutralization by a cross-reactive antibody. *PLoS Pathog* **16**, e1009089 (2020).
- 473 27. B. M. Hauser *et al.*, Engineered receptor binding domain immunogens elicit pan-
474 coronavirus neutralizing antibodies. *bioRxiv*, (2020).
- 475 28. K. Sliepen, T. van Montfort, M. Melchers, G. Isik, R. W. Sanders, Immunosilencing a
476 highly immunogenic protein trimerization domain. *J Biol Chem* **290**, 7436-7442 (2015).
- 477 29. W. F. Garcia-Beltran *et al.*, COVID-19-neutralizing antibodies predict disease severity
478 and survival. *Cell* **184**, 476-488 e411 (2021).
- 479 30. K. H. D. Crawford *et al.*, Protocol and Reagents for Pseudotyping Lentiviral Particles
480 with SARS-CoV-2 Spike Protein for Neutralization Assays. *Viruses* **12**, (2020).
- 481 31. V. D. Menachery *et al.*, SARS-like WIV1-CoV poised for human emergence. *Proc Natl*
482 *Acad Sci U S A* **113**, 3048-3053 (2016).
- 483 32. D. Zhou *et al.*, Evidence of escape of SARS-CoV-2 variant B.1.351 from natural and
484 vaccine induced sera. *Cell*, (2021).
- 485 33. W. F. Garcia-Beltran *et al.*, Circulating SARS-CoV-2 variants escape neutralization by
486 vaccine-induced humoral immunity. *bioRxiv*, (2021).
- 487 34. M. Yuan *et al.*, Structural and functional ramifications of antigenic drift in recent SARS-
488 CoV-2 variants. *bioRxiv*, (2021).
- 489 35. A. G. Schmidt *et al.*, Immunogenic Stimulus for Germline Precursors of Antibodies that
490 Engage the Influenza Hemagglutinin Receptor-Binding Site. *Cell Rep* **13**, 2842-2850
491 (2015).
- 492 36. A. G. Schmidt *et al.*, Viral receptor-binding site antibodies with diverse germline origins.
493 *Cell* **161**, 1026-1034 (2015).
- 494 37. M. J. Moore *et al.*, Retroviruses pseudotyped with the severe acute respiratory syndrome
495 coronavirus spike protein efficiently infect cells expressing angiotensin-converting
496 enzyme 2. *J Virol* **78**, 10628-10635 (2004).
- 497 38. E. Siebring-van Olst *et al.*, Affordable luciferase reporter assay for cell-based high-
498 throughput screening. *J Biomol Screen* **18**, 453-461 (2013).
- 499